Macromolecular Materials and Engineering
www.mme-journal.de

Optimizing the Power Production in an Osmotic Engine via Microfluidic Fabricated and Surface Crosslinked Hydrogels Utilizing Fresh and Salt Water

*Amir Jangizehi, Christian Fengler, Lukas Arens, and Manfred Wilhelm**

Salinity gradients between seawater and river water is a renewable source of energy having a worldwide potential capacity of about 3.1 TW. This energy can be extracted by e.g., an osmotic engine, using hydrogels with high water uptake capacity. Consecutive exposing hydrogels to fresh and saline water makes swelling–shrinking cycles, which can be utilized to move a piston in an osmotic engine. The production of power with this method is significantly suppressed by gelblocking, where voids between particles are blocked so that the water flow is limited and the absorbency significantly retarded. To improve the power production, the gelblocking is minimized within this article by using spherical mono-dispersed hydrogels made by microfluidic technique. In this study mono-disperse poly(acrylic acid-*co*-sodium acrylate) hydrogels with varying diameters (100-600 µm) and varying degrees of neutralization (DN = 10–75 mol%) are synthesized. In addition, hydrogels with different DN are utilized for additional surface crosslinking to fabricate core–shell particles. The maximum power of 0.67 W kg^{-1} is obtained for hydrogels with a diameter of 105 µm, degree of crosslinking (DC) = 1.7 mol%, DN = 75 mol%, and a core-shell architecture, which is three times higher compared to hydrogels having undefined size without a core–shell framework.

1. Introduction

Production of energy from renewable sources is developing due to the rising global energy demand, climate change, and economic growth.[1] In 2016, 19.3% of the global energy consumption and 24.5% of the electricity generation were supplied from renewable sources, and this is predicted to increase to 30% in 2023.[2,3]

Salinity gradients between seawater and river water is one of the renewable sources of energy in nature, which is available at river deltas close to the seas.[4] This energy is considered as a type of marine energy[5] (blue energy) and in contrast to photovoltaic or wind, its extraction depends significantly less on fast changing weather conditions. The global amount of salinity gradient energy capacity is estimated to be 3.1 TW.[6] The extraction of this energy can be accomplished with different methods, such as pressure-retarded osmosis and reversed electro dialysis, by using membranes.[7,8] One major issue associated with these methods is still the relative high cost, ≈0.2–0.6 € kWh^{-1}.[9,10] While the first prototype of an osmotic power plant based on membrane became operational in 2009,[11] the planned commercialization was cancelled in 2013 due to the low economic efficiency. Another major issue with the membrane based methods is the requirement of expensive maintenance, due to fouling and clogging of the membranes over time.[12,13] To overcome these challenges a new approach to extract energy from salt gradients has been introduced by using superabsorbent polymers in an osmotic engine.[14–18] This method can be considered as the inverse of desalination process based on superabsorbent polymers.[19–24] Superabsorbent polymers are charged hydrogels with a high capacity of water uptake, up to 10–1000 times of their own weight.[25–34] The thermodynamic driving force for swelling of hydrogels in water is an osmotic process, where the water is transported from a region of higher chemical potential, the surrounding media, to a region of lower one inside the hydrogel.[35–37] The presence of ions within water reduces the chemical potential difference between hydrogel and surrounding water. Therefore, the equilibrium swelling degree of a hydrogel, Q_{eq} = mass of adsorbed water/mass of dried hydrogels, in saline solution is typically 2–12 times lower than desalinated water.[38] Therefore, the alternating exposure of superabsorbent polymers to fresh and saline water in an osmotic engine leads to swelling–shrinking cycles and the reciprocation motion of the piston (see **Scheme 1**).[17,18] There are three major advantages to produce energy by this approach: i) superabsorbent polymers are inexpensive, typically 1–3 € kg^{-1}, and already utilized and produced at large scale (≈3 MMT per year) in industry as used, e.g., in hygiene applications.[39] ii) The swelling and shrinking cycles in water with different salinity can be repeated several times without the

Dr. A. Jangizehi[+], C. Fengler, Dr. L. Arens, Prof. M. Wilhelm
Institute for Chemical Technology and Polymer Chemistry
Karlsruhe Institute of Technology (KIT)
Engesserstraße 18, Karlsruhe D-76131, Germany
E-mail: manfred.wilhelm@kit.edu

The ORCID identification number(s) for the author(s) of this article can be found under https://doi.org/10.1002/mame.202000174.

[+]Present address: Institute of Physical Chemistry, Johannes Gutenberg-University of Mainz, Duesbergweg 10-14, Mainz D-55128, Germany

DOI: 10.1002/mame.202000174

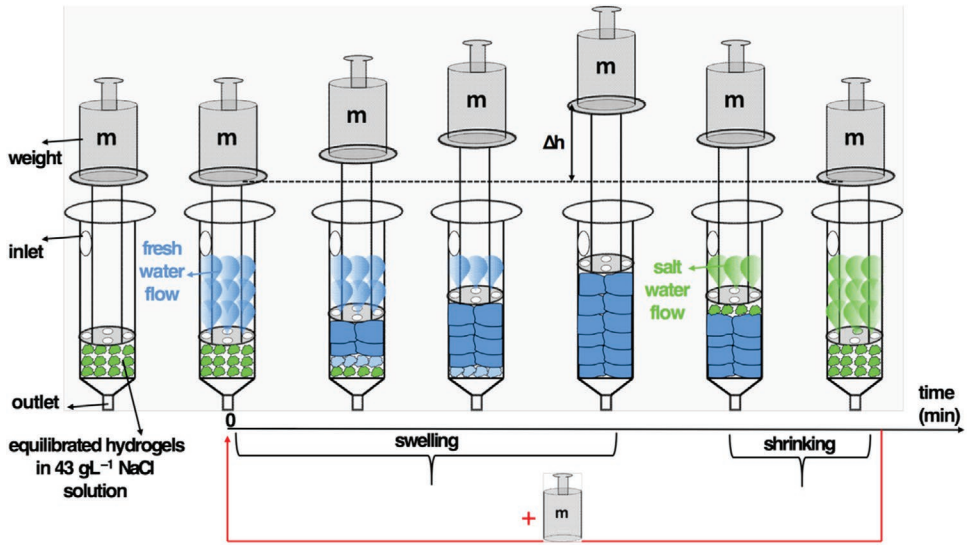

Scheme 1. A) The sketches show an osmotic engine experiment using a syringe type setup. Before starting the swelling–shrinking cycles, the hydrogels are equilibrated overnight in a 43 g L^{-1} NaCl solution with similar ionic strength as seawater. In swelling step, deionized water (DI water) is injected into the syringe for 15 min, while height of the piston is recorded every 2 min. Subsequently, the shrinking process is carried out using NaCl solution (43 g L^{-1}) for 5 min. More weight is added on the piston and the swelling–shrinking cycles are repeated several times until no swelling is observed. The power output is calculated as a function of swelling time, applied pressure and height of the piston using Equation (1). By swelling of the first hydrogel layers, voids between the particles are filled, blocking water flow to the inner hydrogel layers (see the third and fourth sketches from the left). This kinetics hindrance of water absorbency is referred to as gel blocking.

requirement for cleaning.[18] iii) River deltas as a source of fresh and salt water with salt gradient are directly available in different regions.[40] Furthermore, the energy production is emission-free and independent of fast changing weather conditions.

The average power production, P, in any piston engine, which is lifting mass m by a height h within a time t is defined by

$$P = (m \times g \times h)/t \quad (1)$$

where g is the gravity of the earth (9.807 m s^{-2}). In a general view, power is controlled by the capacity of swelling in fresh and saline water (as their ratio controls the change of piston height h), and by the kinetics of swelling to lower t, and its reduction by the addition of mass respective applied pressure. These properties are highly influenced by the hydrogel synthesis parameters, such as the degree of crosslinking (DC) and the degree of neutralization (DN). Arens et al. studied systematically a series of poly (acrylic acid-*co*-sodium acrylate) hydrogels in an osmotic engine, while varying the mentioned synthetic parameters. The maximum power, 0.23 W kg^{-1}, was obtained by hydrogels with DC = 1.7 mol% and DN = 10 mol%.[18] Furthermore, a high influence of the hydrogel size on the power output was observed, in agreement with previous studies.[17] In this previous work, the dried hydrogels were ground and fractionated into three subgroups with sizes of <370, 370–670, and >670 µm in diameter. These particles had an undefined shape and a broad size distribution. The fastest swelling–shrinking cycles were found for particles with diameters of 370–670 µm. The reason for this particle size being best was a compromise between the fast swelling of smaller particles and a low degree of gel blocking of larger particles. Gel blocking is an often reported phenomenon and one of the major concern in hygiene products, which means that water cannot flow inside the inner hydrogel particles due to the blocking of voids and channels between them (see Scheme 1).[41,42] Hence, the power output is lowered significantly due to the prolongation of the swelling step.[18]

Gel blocking can be reduced by maximizing the void space between hydrogels by using spherical particles with a small size distribution. One of the well-known methods to fabricate such monodisperse particles is the droplet-based microfluidic technique.[43–47] In this method, an emulsion of two immiscible fluids is made by the periodic breakup of the first fluid stream via flow focusing of the second, immiscible fluid. As a result, droplets of the first fluid, dispersing in the second one are formed with a highly regular and defined size.[48] If the dispersed phase consists of monomer, crosslinker and initiator, the polymerization of droplets results in the fabrication of microgels.[49] Another method to reduce gel blocking is using core–shell particles, which have a loosely crosslinked core and a higher DC at their shell.[26] The higher crosslinking density at the shell increases the mechanical stability of the hydrogel and makes the particle stiffer without drastically reducing the absorbency. Therefore, these surface-crosslinked particles keep their shape and the void spaces even under higher pressures, which minimizes the gel blocking and improves the water transport between them.[50]

In this work, we focus on the improvement of the power production in an osmotic engine by minimizing the effect of gel blocking to reduce the duration of swelling–shrinking cycles according to Equation (1). Therefore, our approach utilizes monodisperse spherical hydrogels and surface crosslinked, monodispersed particles. For this purpose, three series of poly(acrylic acid-*co*-sodium acrylate) microgels are prepared. First, monodisperse particles with different diameters are

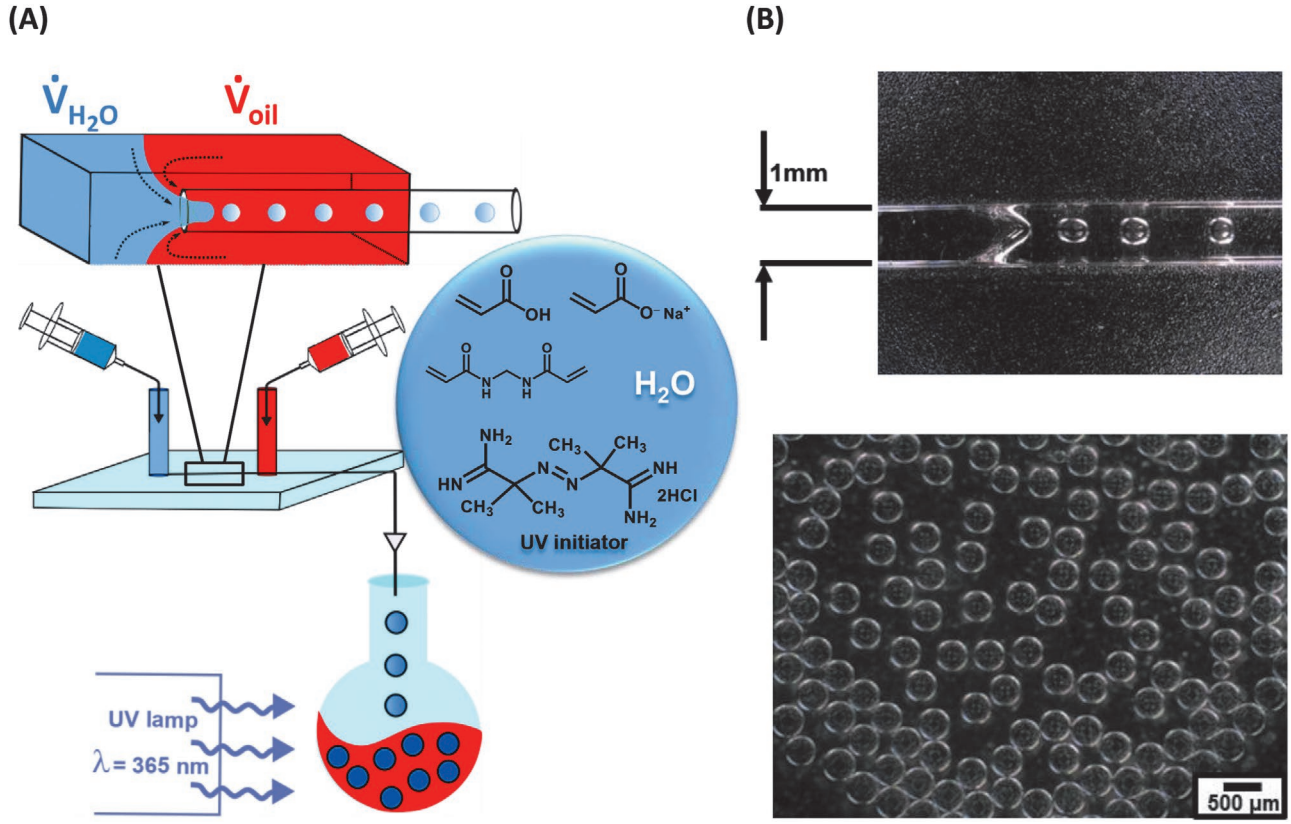

Scheme 2. A) Fabrication of hydrogel particles by the microfluidic technique using glass capillary setup. B) Typical example of the droplet formation in the capillary device. The droplets are spherical and have a monodisperse size distribution.

prepared by the microfluidic technique. Second, spherical particles with almost similar particle size and DC are prepared with microfluidic where the degree of neutralization is varied and subsequently further crosslinked to obtain core–shell hydrogels. The swelling properties of the microgels and their power production in the osmotic engine are studied.

2. Results and Discussion

2.1. Preparation of Hydrogels

Hydrogels with a defined diameter and a narrow size distribution are prepared by the glass capillary microfluidic setup. A drawing of the device and the steps of the microgel preparation are shown in **Scheme 2**. Droplets of the water phase are formed at the intersection of the round and square capillaries by the flow focusing of the oil phase. The size of the droplets is controlled by the flow rates of the dispersed and continuous phases as well as by the diameter of the round capillary tip. The maximum possible flow rates are limited by the diameter of the round capillary tip since merging of droplets has to be avoided. Considering these limitations, six microfluidic experiments were designed to control the size of the final microgels. In these experiments, the flow rate of the dispersed phase is varied between 1.2 and 17 mL h^{-1} and the diameter of the round capillary tip is varied between 0.1 and 1.4 mm. The ratio of the flow rates of the two phases is kept constant at about 3 in all experiments, since with this ratio the amount of oil phase is enough to stabilize the spherical shape of the droplets during polymerization. Using these parameters, microgels are prepared with a diameter ranging from 100 to 700 µm in the dry state. The experimental parameters are summarized in **Table 1**.

Three series of samples are prepared according to the described procedure. In the first series, a focus is given on the

Table 1. Experimental parameters of microfluidic experiments to fabricate microgels with different diameters.

Oil phase flow rate [mL h^{-1}]	Water phase flow rate [mL h^{-1}]	Capillary inner diameter[a)] [mm]	Tip inner diameter [mm]	Particle diameter in the dry state (D_0) [µm]
20	5.6	1.4	1.4	624 ± 43
60	17	1.4	1.4	567 ± 51
60	17	1.4	0.4	485 ± 15
8.5	2.4	0.58	0.58	234 ± 9
17	4.8	0.58	0.58	211 ± 4
4.3	1.2	0.58	0.1	105 ± 6

[a)]The particle size is controlled by the tip diameter of the round capillary at its intersection with the square one. To avoid merging of the particles during fabrication, the maximum possible flow rates cannot be higher than a threshold, which is determined by the diameter of the round capillary tip.

Table 2. Overview of the hydrogel samples used in this work and their equilibrium swelling in DI water Q_{eq}^{DI} and 43 g L^{-1} NaCl solution Q_{eq}^{NaCl}.

Sample[a)]	DC [mol%]	DN [mol%]	Surface crosslinking [vol%]	Q_{eq}^{DI} [g g^{-1}]	Q_{eq}^{NaCl}[b)] [g g^{-1}]	$Q_r = Q_{eq}^{DI}/Q_{eq}^{NaCl}$
105_10_0	1.7	10	0	36.43 ± 0.58	3.46 ± 0.20	10.53
234_10_0						
624_10_0						
485_10_0						
485_25_0	1.7	25	0	54.19 ± 0.89	5.62 ± 0.64	9.64
485_75_0	1.7	75	0	78.55 ± 1.03	16.52 ± 1.36	4.75
485_10_10	1.7	10	10	10.42 ± 0.44	2.32 ± 0.27	4.49
485_25_10	1.7	25	10	14.22 ± 0.47	4.28 ± 0.30	3.32
485_75_10	1.7	75	10	16.44 ± 0.44	7.76 ± 0.84	2.12
105_75_10						

[a)]The samples are designed as *X_Y_Z*, where *X* is average diameter in µm, *Y* is the degree of neutralization, and *Z* is the volume percentage of surface crosslinking ($DC_{total} \approx 9$ mol%); [b)]This solution has identical ionic strength as seawater.

particles size. Hydrogels with the average diameters of 105, 234, and 624 µm are prepared by adapting different capillary diameters and flow rates (see Table 1). In this first series, DC and DN are kept constant at 1.7 and 10 mol%, respectively. The values of DC and DN were selected according to the optimum values, which are reported in previous work.[18] In the second series, samples with a varying DN of 10, 25, and 75 mol% are prepared. These hydrogels have a crosslinking density of 1.7 mol% and an average diameter of 485 µm. A fraction of each sample from the second series is additionally surface crosslinked as described in detail in the Experimental Section. These three series of samples are summarized in **Table 2**. In addition, as a reference sample, hydrogels with DC = 1.7 mol%, and DN = 10 mol%, but with an undefined shape and a broad size distribution is synthesized as described elsewhere.[18] With these samples, we can study and optimize the diameter of the hydrogel particles, and the surface crosslinking to maximize power production in the osmotic engine. As compared to the former synthesis,[18] a main effect is to reduce gel blocking (see **Figure 1**).

2.2. Swelling Properties

The swelling kinetics of the microgels depends strongly on the particle size. This dependency is studied for the first series of samples with varying particle size by optical microscopy (**Figure 2**A,B). It is found that the increase of the microgels diameter upon swelling can be described by a first-order kinetics, as shown in Figure 2C. This swelling is empirically described by[51]

$$D/D_0 = 1 + (D_\infty - D_0)/D_0 \times (1 - \exp(-t/\tau)) \quad (2)$$

in which D is the diameter of the swelling particles at time t, D_0 is the diameter of the hydrogels in the dry state, D_∞ is the equilibrium diameter, and τ is the characteristic time of the swelling process. A smaller τ corresponds to a faster swelling kinetics. In the first series, the values of τ = 0.30, 1.11, and 5.19 min are determined for the characteristic swelling time of the particles with a dry diameter of 105, 234, and 624 µm, respectively (see Figure 2). According to the theory of swelling kinetics of gels proposed by Tanaka,[52] the characteristic swelling time is proportional to the radius squared of the particles in the swelling equilibrium state and the inverse of diffusion coefficient of the hydrogel network. In the first series of the samples, DC and DN are kept similar. Therefore, these hydrogels have almost identical network's diffusion coefficients. As shown in Figure 2D, the characteristic swelling times for these samples show the predicted linear dependency on their equilibrium diameter squared, which is in agreement with the prediction of the theory.

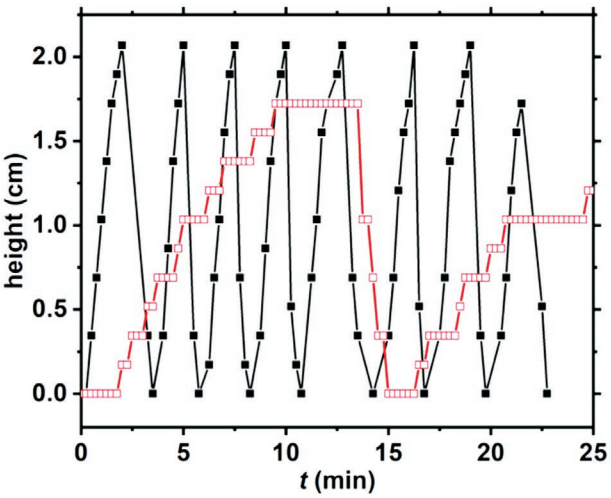

Figure 1. Height of the piston of the osmotic engine as a function of time during consecutive swelling–shrinking cycles using a pressure of 2500 Pa on hydrogels with DC = 1.7 mol% and DN = 10 mol%. Filled, black squares denote spherical samples with D_0 = 105 µm and 10 vol% of additional surface crosslinking. Open, red squares indicate hydrogels with undefined shape and a large size distribution between 370 and 670 µm. The slow kinetics of undefined particles is obvious.

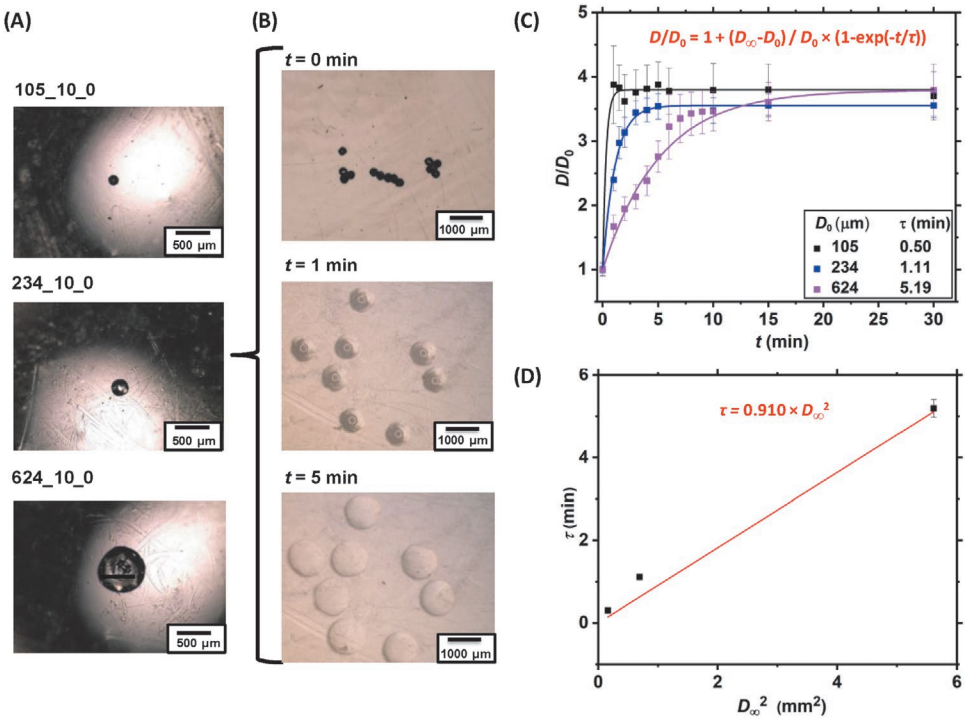

Figure 2. A) Observation of microgels with different diameters by the reflective microscope. B) Study of swelling kinetics for the sample 234_10_0 in fresh water. Snapshots are taken in defined time intervals and the particle diameters are analyzed with the microscope software. For each data point, the error bar is determined by measuring diameters of multiple particles (at least 8). C) The swelling data for the first series of the samples are fitted with a first-order kinetics. D) The characteristic swelling time obtained from this fitting is plotted versus diameter squared in the equilibrium swelling state. The data show a linear dependency, which is in agreement with the swelling kinetics theory of Tanaka.[52]

The swelling kinetics is studied for the second series of samples with D_0 = 485 µm and different degrees of neutralization. By fitting Equation (2), values of 4.85, 4.63, and 2.53 min are found for particles with DN = 10, 25, and 75 mol%, respectively (see Figure S1 in the Supporting Information). This result illustrates that similar to Q_{eq}, the swelling kinetics depend on the amount of charged groups along the polymer backbone, and is faster for particles with higher DN. This may originate from an increased difference in the osmotic pressure between hydrogel and surrounding water. Furthermore, the hydrophilic nature of the polymer chains increases with the amount of charged groups.

2.3. Power Production in the Osmotic Engine

In the osmotic engine experiment (see Scheme 1), the fresh water flows into the syringe type osmotic engine for 15 min, to induce swelling of the hydrogels. In this step, height of the piston is recorded every 2 min (swelling time = 2, 4, 6, 8, 10, 12, 14, and 15 min). After this time, the inlet is replaced with NaCl solution (43 g L^{-1}) for 5 min to make the hydrogels shrink, which moves the piston back to the initial height. After that, a new weight is added to the piston and the described swelling–shrinking cycle is repeated again. For each sample, at least eight different masses, which apply a pressure between 184 and 15000 Pa on the hydrogels is examined. Therefore, a set of (power, time, and pressure) data is obtained for each sample. In a 2D data presentation, the power is plotted versus time for different applied pressures or is plotted versus pressure for different recording times in the swelling step. As a typical example, for hydrogels with an undefined shape and a broad size distribution (average diameter of 370–670 µm), DC = 1.7 mol%, and DN = 10 mol%, the results of osmotic engine experiments are presented in **Figure** 3A. The data can also be presented in a 3D format, in which the variation of the power by time and pressure and the maximum power is more comprehensible (Figure 3B). The osmotic engine experiment is performed for the three synthesized series of samples to investigate the influence of particle size as well as the effect of surface crosslinking of the hydrogels on the power production.

2.3.1. Influence of Particle Size

For the first series of samples (constant DC, DN, and varying particle diameter), the produced power versus time and pressure is shown in **Figure 4**. In these samples, the maximum power outputs (P_{Max}) are consistently higher compared to the power produced by the hydrogels with similar DC and DN but with undefined shape and a broad size distribution (see Figure 3). In addition, P_{Max} increases with decreasing particles size. The highest power output of 0.54 W kg^{-1} that this series generates is obtained by using the hydrogel sample

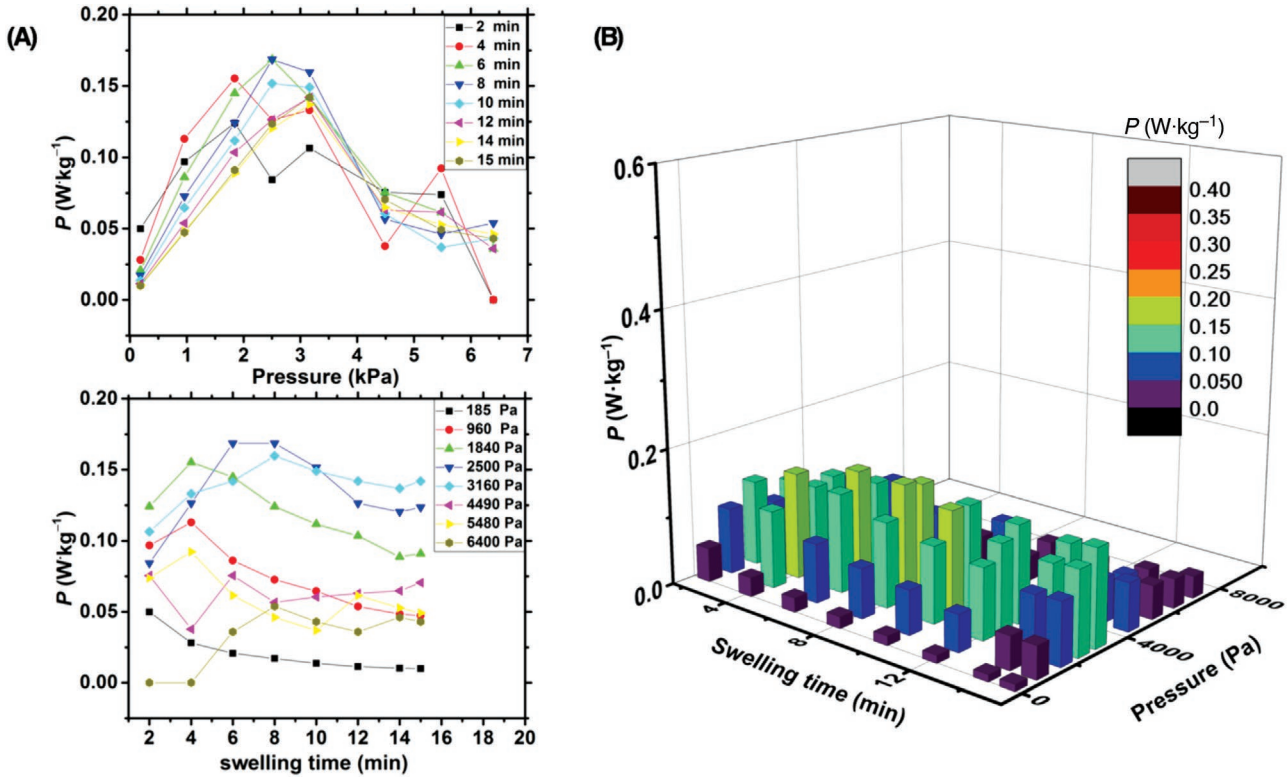

Figure 3. The results of the osmotic engine experiment as a series of (power, pressure, and time) data. These results can be plotted in A) 2D or B) 3D format. The presented data here are the results of hydrogels with a large size distribution, 370–670 µm, and undefined shape.

105_10_0 (D_0 = 105 µm). This value is 1.35 and 3 times larger than produced by particles with a diameter of 234 and 624 µm, respectively (Figure 4D). This variation originates from the systematically decreasing of the time at which P_{Max} is obtained by decreasing the particles diameter. The time corresponded to P_{Max} is much higher than the associating variation of τ (3–4-fold of τ) due to the additionally applied pressure in the osmotic engine. However, the trend is similar to τ. The time corresponding to P_{Max} is increasing with the microgel diameter, and is shorter for smaller particles. This means that applying pressure on monodispersed spherical hydrogels does not change the dependency of their swelling kinetics on the particles size. One explanation for this result could be the presence of enough effective voids between particles, which minimizes gel-blocking effect during osmotic engine experiments

2.3.2. Influence of Surface Crosslinking

The osmotic engine experiment is also performed for the hydrogels of the second series: constant DC, D_0, and varying DN and for the third series: constant DC, D_0, and 10 vol% of surface crosslinking of hydrogel samples. According to the results of the first series, the maximum power is obtained by the hydrogel with a diameter of D_0 = 105 µm. However, the second and third series samples are prepared by the average diameter of 485 µm with microfluidic, since the fabrication rate of hydrogels with such diameter is about fourteen times higher than that of particles with D_0 = 105 µm (see Table 1). Consequently, the fabrication process of the hydrogels with larger diameter allows easing for study the effect of surface crosslinking. Therefore, D_0 = 485 µm is used with this assumption that changing particle size does not change the effect or relative trend of DN or surface crosslinking on the power production. By varying the degree of neutralization, the power output decreases with DN and the maximum power production is obtained for hydrogels with DN = 10 mol% (Figure S2 in the Supporting Information). This observation could be related to the increasing Q_{eq} by increasing DN (vide supra), which decreases the mechanical strength of the hydrogels (Figure S3 in the Supporting Information). Therefore, these samples may deform more under pressure compared to the hydrogels with lower DN, and thus may still have significant gel blocking during swelling. By surface crosslinking, no mechanical power production could be obtained for the sample 485_10_10. This is at first surprising, but could be explained by the low Q_{eq} of this sample in DI water. By increasing DN, Q_{eq} increases and performing osmotic engine experiment is possible for the samples 485_25_10 and 485_75_10. In opposite to the corresponding samples of the second series, increasing DN for the surface-crosslinked hydrogels has a positive effect on the maximum power output (**Figure 5**). This is explained by the high influence of surface crosslinking on boosting mechanical strength of the microgels (see Figure S3 in the Supporting

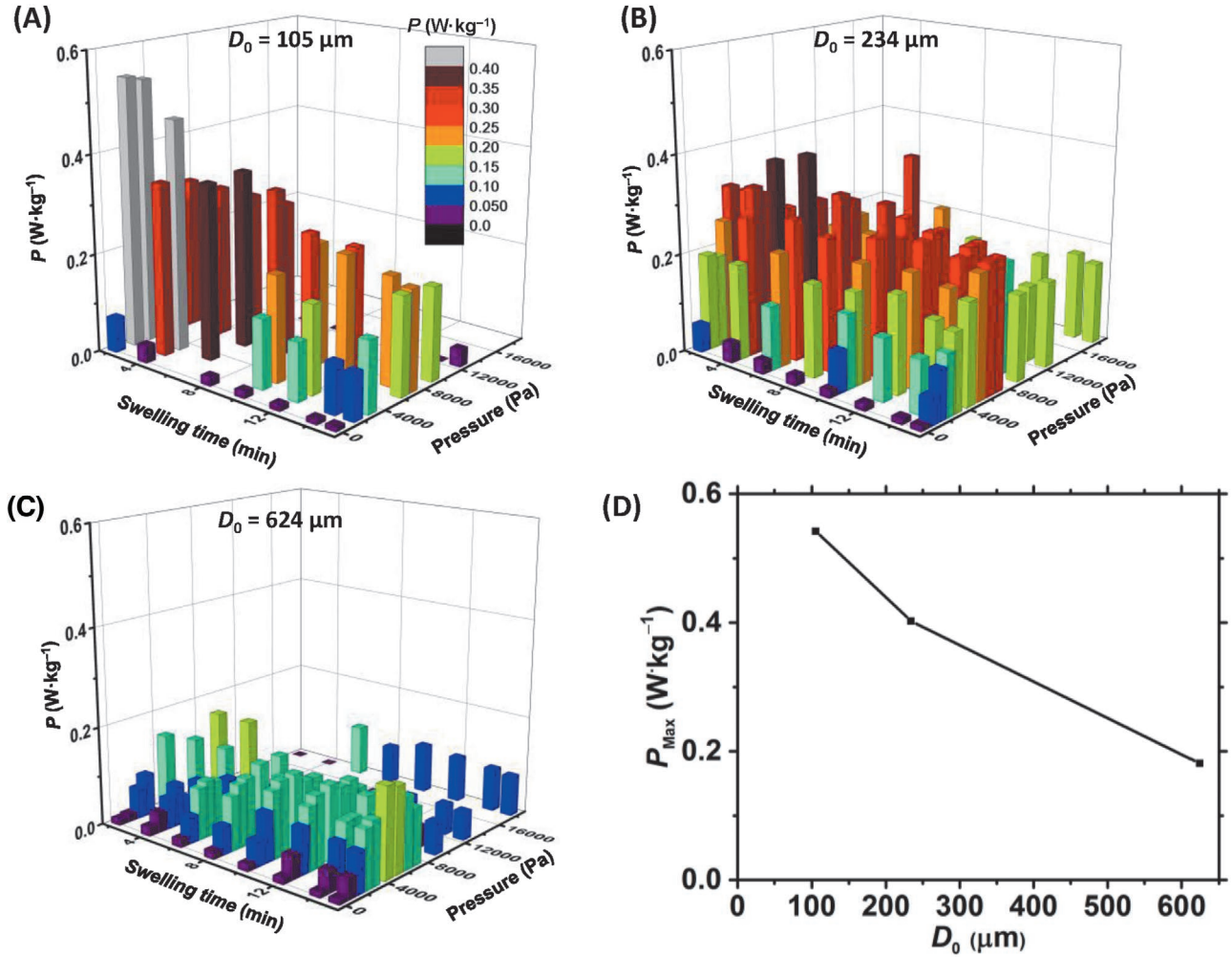

Figure 4. Mechanical power production in the osmotic engine using spherical poly(sodium acrylate-*co*-acrylic acid) hydrogel particles as a function of time and applied pressure. The hydrogels are fabricated by the microfluidic technique with DC = 1.7 mol% and DN = 10 mol%. The average dry particle diameters are A) 105 µm, B) 234 µm, and C) 624 µm. The variation of the maximum power as a function of hydrogel particle diameter in the dried state is presented in panel (D).

Information). The hydrogels with high mechanical strength keep their shape under pressure, and consequently have a much low gel-blocking effect. This also explains that the pressure at which the maximum power is obtained is much larger than that of associated precursor samples.

Comparison of the second and third series of samples shows that the sample 485_75_10 has a higher P_{Max} than sample 485_10_0 (0.32, 0.22 W kg^{-1}, respectively). Therefore, we conclude that 75 mol% as a degree of neutralization and 10 vol% of additional surface crosslinking are optimized structure parameters to have maximum mechanical power production. Consequently, by recalling the result of the first series, which showed that an increase of mechanical power is achieved by decreasing the particles diameter, we assume that spherical hydrogels with the characteristics: D_0 = 105 µm, DN = 75 mol%, and 10 vol% of surface crosslinking should lead to further improved power production. To confirm this assumption, hydrogel particles are prepared according to these parameters with the microfluidic technique and the power output is investigated. The results show that with such a hydrogel, a maximum power of 0.67 W kg^{-1} is obtained (see **Figure 6**), which is a further 24% improvement in the maximum power in comparison to the maximum power output by the first series samples.

2.3.3. Effect of Swelling and Mechanical Properties on Power Production

Considering the mechanism of the piston movement related to amplitude and time in the proposed osmotic engine suggest that it correlates with swelling as well as mechanical properties of the hydrogel samples. We assume that Q_r (ratio of swelling in DI water to salt solution) and the characteristic swelling time are directly proportional to h and t in Equation (1). In addition, hydrogels with high mechanical strength (high modulus, G'; see Figure S3 in the Supporting Information) keep their shape under load, which improves water

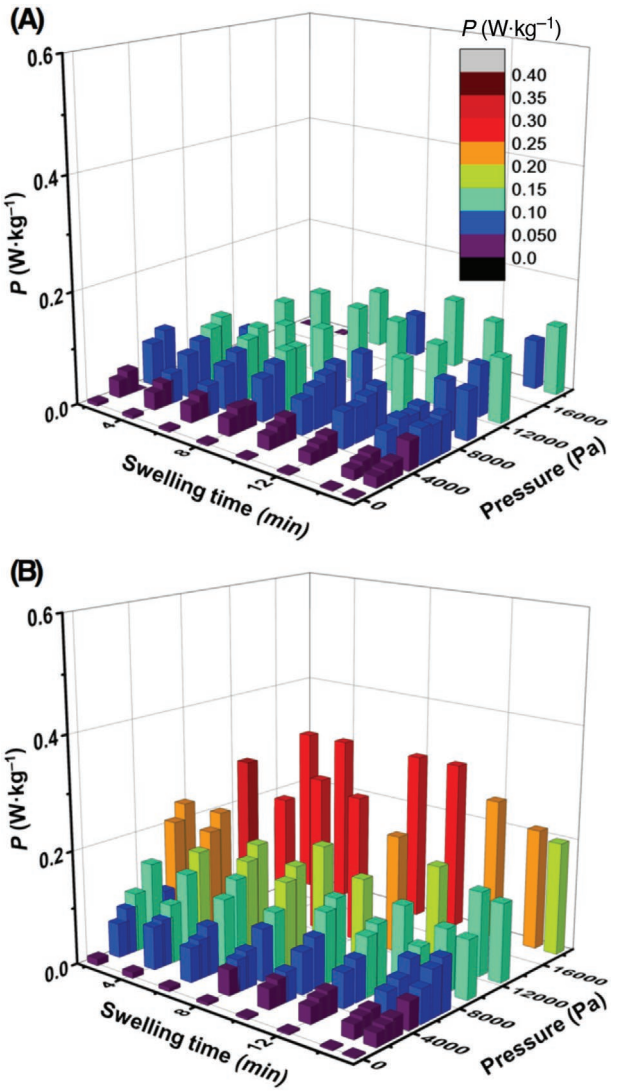

Figure 5. Power production in the osmotic engine using core–shell spherical poly(sodium acrylate-*co*-acrylic acid) hydrogels. The hydrogels are prepared in two steps. In the first step, the hydrogels with an average diameter of 485 µm and DC = 1.7 mol% are fabricated by the microfluidic technique. The degree of neutralization is A) 25 mol% or B) 75 mol%. In the second step, 10 vol% of these hydrogels is fully crosslinked as described in the experimental section.

flow between them. Therefore, we assume that the power production in the employed osmotic engine scales with the product of Q_r, $1/\tau$, and G', if additional effects, such as gel blocking are neglected.

Interestingly, plotting the achieved values of power production for all samples versus $\log(Q_r \times 1/\tau \times G')$ shows a linear dependency, with a slope of about 0.3 as observed in **Figure 7**. In an approximation, this plot might be employed to predict the efficiency of a hydrogel with known swelling and mechanical properties to words its performance in an osmotic engine. However, it should be noted that the fitting parameters will obviously additionally depend on monomer type, network architecture and network heterogeneity.

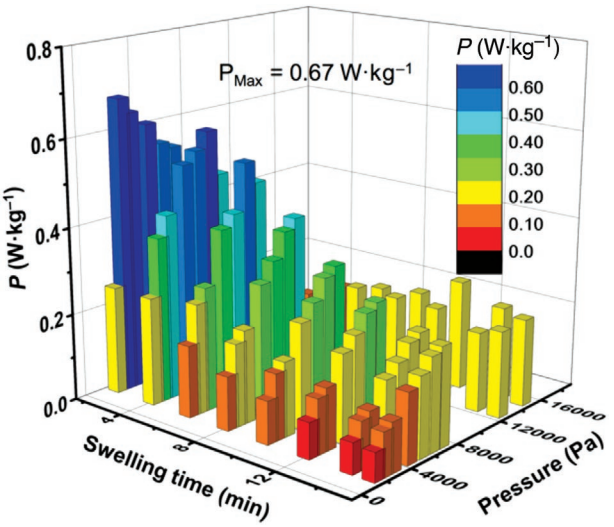

Figure 6. Power production in the osmotic engine using spherical poly(sodium acrylate-*co*-acrylic acid) hydrogels with D_0 = 105 µm, DC = 1.7 mol%, and DN = 75 mol% and 10 vol% of surface crosslinking.

2.3.4. Power Production Using Model Seawater with Multivalent Ions

For a real application as explained in the introduction, the osmotic engine should be examined with seawater instead of saline solution. So far, we utilized NaCl solution with the concentration of 43 g L^{-1}, since this concentration has almost identical ionic strength as seawater.[53] In addition to Na^+, seawater contains multivalent cations such as Ca^{2+} and Mg^{2+}, which may induce a collapse of poly(acrylic acid-*co*-sodium acrylate) hydrogels, due to their strong interaction with charged groups, as shown in previous work.[16,54] Therefore, during the continuous operation of swelling and shrinking cycles in the osmotic engine, hydrogels may lose

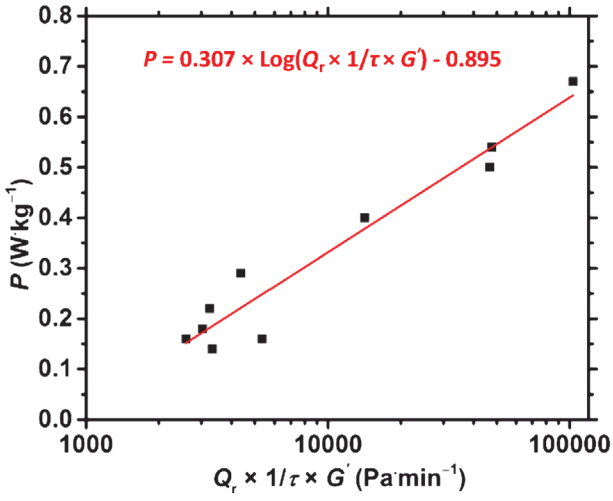

Figure 7. For each sample in this work, the power is plotted versus figure of merit of Q_r, $1/\tau$ (min^{-1}) and G' (Pa). With an approximation, a slope of 0.3 as a function of $\log(Q_r \times 1/\tau \times G')$ is fitted on the data.

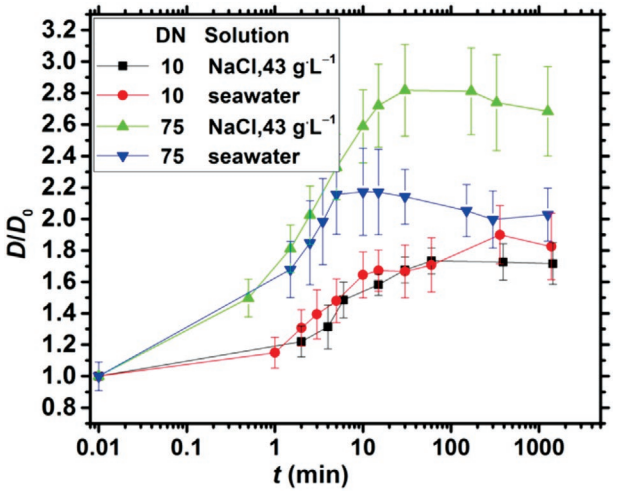

Figure 8. Swelling kinetics of hydrogels with DN = 10 mol% or DN = 75 mol% in 43 g L^{-1} NaCl solution, and a model seawater containing Ca^{2+} and Mg^{2+}. The diameter of the particles is calculated using the microscope as described in the Experimental Section. The dry diameter of the hydrogels is D_0 = 485 µm.

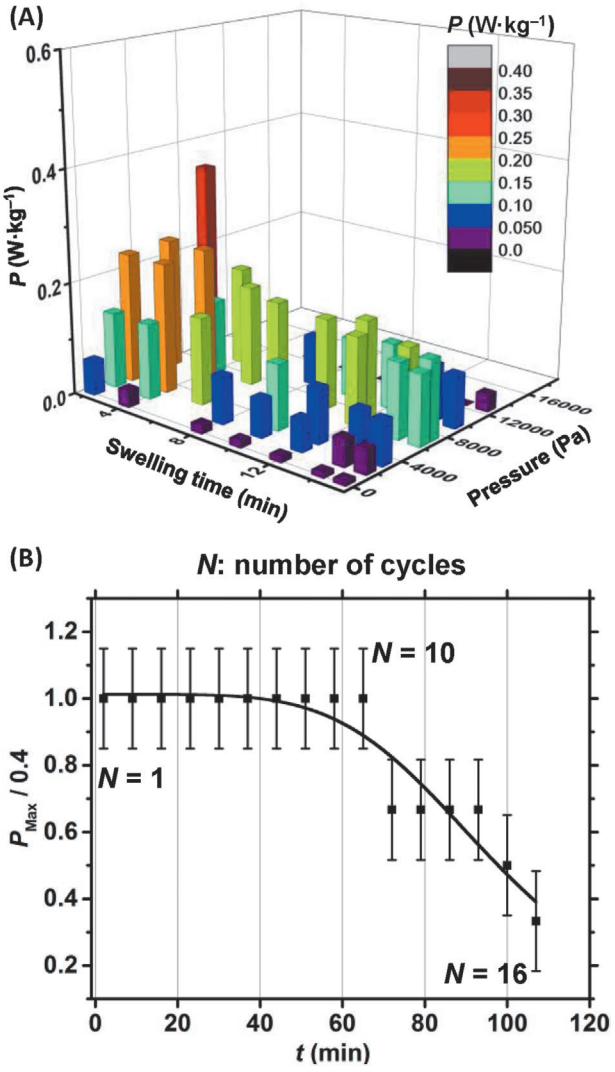

Figure 9. A) The result of osmotic engine experiment for sample 105_10_0 in the model seawater. B) Repeating swelling–shrinking cycles with this sample. The pressure and the swelling time of this experiment are selected according to the data of panel (A). P_{Max} is the maximum power of each cycles. 0.4 W kg^{-1} is the maximum power of the first cycle. The error bars are determined based on the minimum readable height in the syringe osmotic engine. The line is a guide for the eyes.

their swelling capacity over time in real seawater. The sensitivity of Q_{eq} to multivalent cations should depend strongly on the ratio of charged groups along the polymer segments. In order to verify this hypothesis, we studied the swelling kinetics of samples 485_10_0 and 485_75_0 in NaCl solution and a model seawater containing 2.4 wt% NaCl, 0.52 wt% $MgCl_2$, and 0.12 wt% $CaCl_2$[53] by the optical microscope (**Figure 8**). These experiments were run for about 24 h to evaluate the possible variation of Q_{eq} for seawater at long time periods to investigate the influence of multivalent cations. The sample with a large charge fraction of DN = 75 mol% displays a continuous increase of D/D_0 over the first 13 min of the experiment in saline solution with no reduction in swelling capacity in the remaining time of the experiment (Figure 8). The swelling behavior of 485_75_0 in model seawater, however, is significantly different. The ratio of D/D_0 is increased only in the first 3 min of the experiment. Then, D/D_0 is almost constant between t = 3 and 15 min. Afterward, the swelling capacity of the sample is gradually decreased up to t = 5 h and finally D/D_0 reaches an equilibrium value. The equilibrium ratio of D/D_0 in model seawater is about 25% lower of that in saline solution. In contrast, the swelling kinetics and Q_{eq} of the sample with only 10 mol% of charged groups show no significant difference in saline solution and model seawater, as the lower amount of charged groups might be reduce the probability of interactions via divalent cations.

This similarity between swelling behavior of the sample with a DN of 10 mol% in NaCl solution and model seawater encourages us to examine this hydrogel in the osmotic motor using model seawater instead of 43 g L^{-1} NaCl solution. We select sample 105_10_0 for this experiment. The results are shown in **Figure 9**A. The average power production with model seawater is smaller than with NaCl solution, specifically in the time range of 2–6 min. The maximum power is 0.4 W kg^{-1}, which is 70% of the obtained value in the corresponding experiment with NaCl solution. Another important factor in real applications is the long-time resistance of the power production without replacing of hydrogels. Therefore, swelling–shrinking cycles are repeated over 2 h in model seawater using the optimum time and pressure values where the maximum power was observed (2 min and 9500 Pa, respectively). The power of each cycle, normalized to the initial value of 0.4 W kg^{-1} is plotted against time in Figure 9B. This ratio is almost constant within the first ten cycles, but starts to decrease afterward. This result shows that even by using hydrogels with a low DN, additional effects such as interaction of multivalent ions and charged groups reduce the power output over time.

3. Conclusion

The extraction of renewable energy from water salinity gradients can be accomplished by using superabsorbent polymers in an osmotic engine. In this study we have shown that the power production with this method can be improved by reducing the gel-blocking effect, which is a known common effect for hydrogels with high swelling capacity. Hydrogel particles deform under pressure and fill the void between particles, which hinders the flow of additional water into the particles and drastically reduces absorption capacity.

Two strategies have been investigated to tackle this disadvantage: i) preparation of spherical monodisperse hydrogels by the microfluidic technique and ii) increasing stiffness of the microfluidic hydrogels without decreasing drastically their swelling capacity under pressure via surface crosslinking. We prepared three series of samples varying by the parameters: particle size D_0, degree of neutralization, DN, and surface crosslinking. We found that spherical hydrogels with a diameter of 105 µm, DC = 1.7 mol%, DN = 75 mol%, and core–shell architecture leads to the maximum power up to 0.67 W kg^{-1} of dried hydrogel, when DI water and 43 g L^{-1} NaCl solution are used in the experiment. This value is more than three times greater than for hydrogels with an undefined shape, a large size distribution and without a surface crosslinked shell. We also found that as a good approximation, the power scales as $(Q_r \times 1/\tau \times G')^{0.3}$, where Q_r is the equilibrium swelling ratio between deionized and saline water, τ is the characteristic swelling time, and G' is the elastic modulus of the sample. This semiempirical fitting is possible for spherical particles, if additional effects such as gel blocking can be neglected. By replacing NaCl solutions with a model seawater containing the multivalent cations, Ca^{2+} and Mg^{2+}, a 30% reduction of the power is observed, which could be related to the interaction between the cations and charged groups. The improvement of reusability of the experiment in seawater should be achieved by modifying the chemical composition of the hydrogel, e.g., using cationic monomers.[55] These cationic monomers are the scope of further investigation in our group.

4. Experimental Section

Materials: Acrylic acid (anhydrous, 99%), methylenebisacrylamide (MBA), sodium hydroxide (33 wt% in water), *N*,*N*,*N*′,*N*′-tetramethylenediamine (TEMED), sodium persulfate (99%), 2,2′-azobis(2-methylpropionamidine) dihydrochloride (V50), ethylene glycol diglycidyl ether (EGDE), and paraffin oil (viscosity, η = 25–80 mPa s at 20 °C) were purchased from Aldrich, TCI Chemicals or Karl-Roth and were used without further purification. The surfactant with the trade name ABIL EM 90 (nonionic water/oil emulsifier with a polymeric structure based on silicone; viscosity, η = 1–2.3 Pa s @ 25 °C) was supplied from Evonik Industries.

Microfluidic Device: The glass capillary microfluidic device was made by using a round capillary with the length of 100 mm, inside a square capillary with the length of 75 mm (see Scheme 2). The diameters of the capillaries were chosen to get a perfect coaxial alignment between square and round ones: round capillaries with the (inner, outer) diameters of (0.58, 1) mm or (1.4, 2) mm and square capillaries with the (width, thickness) of (1.10, 0.25) mm or (2.27, 0.53) mm. These capillaries were fixed on a microscope slide with transparent epoxy glue. To supply fluids, two nonsharp needles were utilized. One needle was attached on the tip of the round capillary and another one was placed on the intersection of two capillaries by the epoxy glue.

Preparation of Microgels: Microgels were prepared by using a glass-capillary microfluidic device. The dispersed phase consisted of partially neutralized acrylic acid, water, MBA, and 2,2′-azobis(2-methylpropionamidine) dihydrochloride (V50) as initiator. The weight ratio of water to the monomer was 4 g g^{-1}. This solution was emulsified by flow focusing with paraffin oil containing 10 wt% of surfactant ABIL EM 90 (Evonik industries). The droplets that were dispersed in the oil phase were collected in a beaker and exposed to UV light with a wavelength of λ = 365 nm, for at least 2 h for polymerization. As a typical example for the preparation of microgels with the diameter of 234 µm, DC = 1.7 mol%, and DN = 10 mol%, the crosslinker MBA (0.10 g, 0.68 mmol) were dissolved in 12.35 mL of water. Acrylic acid (2.88 g, 40 mmol) was added to this solution and the mixture was cooled in an ice bath. To partially neutralize acid groups, 0.36 mL of 33 wt% NaOH solution was added dropwise. After that, V50 (0.20 g, 0.72 mmol) was added. For the preparation of the continuous phase, 45 g of paraffin oil and 4.5 g of ABIL EM90 were mixed for 10 min. Both fluids were supplied into the microfluidic device by disposable syringes (BD Pastipak) and polyethylene tubes (Intramedic Clay Adams PE tubing, PE90) using two syringe pumps (Harvard Apparatus, PHD Ultra). The flow rate of the dispersed phase and the continuous phase were 2.40 and 8.50 mL h^{-1}, respectively, which led to the production of maximum ≈7 g dried hydrogels in 8 h. After polymerization by UV light, the microgels were washed five times with isopropanol and five times with deionized water (DI water), and then they were dried at 50 °C under reduced pressure.

Surface Crosslinking: The surface crosslinking of the hydrogels was done by utilizing EGDE as the crosslinker in a mixture of heptane and water. In this work, the ratio of the volume of the (additionally crosslinked) shell to the volume of the core ($volume_{shell}/volume_{core}$) was 0.1, which means that 10 vol% of the particles was additionally crosslinked with EGDE. In other words, the volume fraction of the hydrogels that was penetrated by the surface crosslinker was 10 vol%. This means that, the amount of water that should be utilized in the reaction was 10% of the total amount of water required to reach to the equilibrium swelling degree of the hydrogels: m (water) = 0.1 × Q_{eq} × m (hydrogels). In addition, considering that every EGDE molecule can ideally react with two sodium acrylate (SA) groups in the penetrated area, the required mole of EGDE in the reaction was calculated as n(EGDE) = [n(SA) × 0.1]/2. As a typical example for surface crosslinking of the sample produced by microfluidic with a diameter of 485 µm and DN = 10 mol%, 1 g of this sample (13.5 mmol of SA) was suspended in a mixture of *n*-heptane (40 mL), and sorbitan monolaurate (0.02 g, 0.06 mmol) as the emulsifier. Then, EGDE (0.12 g 0.68 mmol), which was prior dissolved in water (3.6 mL), was added. The suspension was stirred with a magnetic stir bar (≈250 rpm) at 65 °C for 4 h. The hydrogel was filtered and washed five times with DI water and dried at 50 °C under reduced pressure.

Swelling Kinetics of Hydrogels: The swelling kinetics of microgels was studied using a reflective light microscope (Keyence VHX 900F). The dried particles were placed in a small Petri dish and one snapshot was taken as a reference at t = 0. DI water was added to the Petri dish by a pipette and the swelling of the particles was monitored by taking snapshots at defined time intervals (typically 1 min for swelling time of 0–10 min, and 5 min for swelling time of 10–30 min). All photos were analyzed using the internal software of the microscope. The error bar of each analysis represented the standard deviation of diameters of at least eight particles.

Osmotic Engine: A syringe-type osmotic engine was used to study the power production. This syringe had one inlet as well as one outlet (Scheme 1). Before starting the experiment, 250 mg of dried hydrogels was equilibrated in the 43 g L^{-1} NaCl solution. This NaCl solution had almost identical ionic strength as seawater.[53] The hydrogels were placed between two filter papers (mesh size 3–5 µm) and two metal wires (mesh size 120 µm). The deionized water flowed into the engine to induce the swelling of the hydrogels. Fifteen min was considered as

the overall time for the swelling step, and during this time, the height of the piston was recorded every 2 min. In each interval time (at 2, 4, 6, 8, 10, 12, 14, and 15 min), the height of the piston was read and power production was determined according to Equation (1). Then, the inlet flow was replaced with the NaCl solution (43 g L^{-1}) for at least 5 min to make the hydrogels shrink again. After that, a selected weight was added to the piston to increase the pressure, and then the swelling–shrinking cycle was repeated again. The weights that were used in this experiment were 12, 169, 213, 303, 370, 431, 489, 856, and 1010 g, which were placed on the piston of the osmotic engine with a surface area of 6.60 cm^2. Therefore, the power production was measured in the pressure range of 184–15000 Pa.

Rheology: The mechanical properties of hydrogels were studied by measuring their linear viscoelastic responses using a stress-controlled Anton Paar MCR 302 rheometer equipped with 25 mm parallel plate–plate geometry at 25 °C. To avoid water evaporation during measurements, a solvent trap was utilized. For each sample, an amplitude sweep was recorded at a constant frequency (γ = 0.0001–1%, ω = 1 rad s^{-1}) to determine the linear viscoelastic regime. Then, a frequency-sweep experiment was performed at a constant strain amplitude (γ = 0.01%; ω = 0. 1–100 rad s^{-1}).

Supporting Information

Supporting Information is available from the Wiley Online Library or from the author.

Acknowledgements

The authors thank the Vector foundation (https://vector-stiftung.de/) and the DFG (Grant No. WI 1911/24-1) for the financial support. The SFB 1176 is acknowledged for support within project C1. The authors are grateful to Dr. Michael Pollard for proofreading the manuscript. Prof. Dr. Sebastian Seiffert (Johannes Gutenberg-University of Mainz) is kindly acknowledged for providing the possibility of rheology measurements.

Conflict of Interest

The authors declare no conflict of interest.

Keywords

gel blocking, microfluidic devices, osmotic engines, power production

Received: March 15, 2020
Revised: April 29, 2020
Published online:

[1] J. L. Aleixandre Tudó, L. Castelló Cogollos, J. L. Aleixandre, R. Aleixandre-Benavent, *Renewable Energy* **2019**, *139*, 268.
[2] REN21: Global Status Report, REN21, Paris **2016**, https://www.ren21.net/wp-content/uploads/2019/05/REN21_GSR2016_FullReport_en_11.pdf.
[3] Renewables 2018: IEA Market Analysis and Forecast from 2018 to 2023, International Energy Agency, Paris **2018**, https://www.iea.org/reports/renewables-2018.
[4] A. Hussain, S. M. Arif, M. Aslam, *Renewable Sustainable Energy Rev.* **2017**, *71*, 12.
[5] J. Cruz, *Ocean Wave Energy: Current Status and Future Prespectives*, Springer Science and Business Media, New York **2007**.
[6] P. Stenzel, *Energy Sustainability* **2012**, *4*, 643.
[7] N. Y. Yip, M. Elimelech, *Environ. Sci. Technol.* **2012**, *46*, 5230.
[8] D. A. Vermaas, J. Veerman, N. Y. Yip, M. Elimelech, M. Saakes, K. Nijmeijer, *ACS Sustainable Chem. Eng.* **2013**, *1*, 1295.
[9] S. Loeb, *Desalination* **2002**, *143*, 115.
[10] T. T. Tran, K. Park, A. D. Smith, *Energy* **2017**, *126*, 97.
[11] K. Gerstandt, K. V. Peinemann, S. E. Skilhagen, T. Thorsen, T. Holt, *Desalination* **2008**, *224*, 64.
[12] D. M. Warsinger, J. Swaminathan, E. Guillen-Burrieza, H. A. Arafat, *Desalination* **2015**, *356*, 294.
[13] M. H. Dore, *Desalination* **2005**, *172*, 207.
[14] R. Cortese, F. Theeuwes, *US Patent 4327725A*, **1982**.
[15] Y. Osada, H. Okuzaki, H. Hori, *Nature* **1992**, *355*, 242.
[16] F. Horkay, I. Tasaki, P. J. Basser, *Biomacromolecules* **2000**, *1*, 84.
[17] X. Zhu, W. Yang, M. C. Hatzell, B. E. Logan, *Environ. Sci. Technol.* **2014**, *48*, 7157.
[18] L. Arens, F. Weißenfeld, C. O. Klein, K. Schlag, M. Wilhelm, *Adv. Sci.* **2017**, *4*, 1700112.
[19] J. Höpfner, C. Klein, M. Wilhelm, *Macromol. Rapid Commun.* **2010**, *31*, 1337.
[20] L. Arens, J. B. Albrecht, J. Höpfner, K. Schlag, A. Habicht, S. Seiffert, M. Wilhelm, *Macromol. Chem. Phys.* **2017**, *218*, 1700237.
[21] J. Höpfner, T. Richter, P. Košovan, C. Holm, M. Wilhelm, in *Intelligent Hydrogels* (Eds: G. Sadowski, W. Richtering), Springer, Berlin **2013**, Ch. 19.
[22] W. Ali, B. Gebert, T. Hennecke, K. Graf, M. Ulbricht, J. S. Gutmann, *ACS Appl. Mater. Interfaces* **2015**, *7*, 15696.
[23] L. Arens, D. Barther, J. Landsgesell, C. Holm, M. Wilhelm, *Soft Matter* **2019**, *15*, 9949.
[24] H. Mittal, S. S. Ray, M. Okamoto, *Macromol. Mater. Eng.* **2016**, *301*, 496.
[25] M. J. Zohuriaan Mehr, K. Kabiri, *Iran. Polym. J.* **2008**, *17*, 451.
[26] M. Elliott, *Product Development Scentist for SAP*, Vol. 13, BASF Aktiengesellschaft, Ludwigshafen, Germany **2004**.
[27] M. Liu, T. Guo, *J. App. Polym. Sci.* **2001**, *82*, 1515.
[28] K. Buchanan, B. Hird, T. Letcher, *Polym. Bull.* **1986**, *15*, 325.
[29] J. Höpfner, G. Guthausen, K. Saalwächter, M. Wilhelm, *Macromolecules* **2014**, *47*, 4251.
[30] O. Okay, in *Hydrogel Sensors and Actuators* (Eds: G. Gerlach, K.-F. Arndt), Springer, Berlin **2009**, Ch. 1.
[31] L. Arens, M. Wilhelm, *Macromol. Chem. Phys.* **2019**, *220*, 1900093.
[32] F. Cavalli, C. Pfeifer, L. Arens, L. Barner, M. Wilhelm, *Macromol. Chem. Phys.* **2020**, *221*, 1900387.
[33] K. Kabiri, M. J. Zohuriaan-Mehr, *Macromol. Mater. Eng.* **2004**, *289*, 653.
[34] J. Zhang, L. Wang, A. Wang, *Macromol. Mater. Eng.* **2006**, *291*, 612.
[35] P. J. Flory, *Principles of Polymer Chemistry*, Cornell University Press, Ithaca, New York **1953**.
[36] W. Ali, B. Gebert, S. Altinpinar, T. Mayer-Gall, M. Ulbricht, J. Gutmann, K. Graf, *Polymers* **2018**, *10*, 567.
[37] O. Okay, S. B. Sariisik, *Eur. Polym. J.* **2000**, *36*, 393.
[38] A. Katchalsky, I. Michaeli, *J. Polym. Sci.* **1955**, *15*, 69.
[39] K. Kosemund, H. Schlatter, J. L. Ochsenhirt, E. L. Krause, D. S. Marsman, G. N. Erasala, *Regul. Toxicol. Pharmacol.* **2009**, *53*, 81.
[40] T. Xie, X. Liu, T. Sun, *Ecol. Modell.* **2011**, *222*, 241.
[41] H. Wack, M. Ulbricht, *Ind. Eng. Chem. Res.* **2007**, *46*, 359.
[42] H. Wack, M. Ulbricht, presented at First Int. Conf. on Self Healing Materials, Nordwijk aan Zee, The Netherlands, **2007** (accessed: April 2007).
[43] P. Zhu, L. Wang, *Lab Chip* **2017**, *17*, 34.
[44] Z. Z. Chong, S. H. Tan, A. M. Gañán-Calvo, S. B. Tor, N. H. Loh, N.-T. Nguyen, *Lab Chip* **2016**, *16*, 35.
[45] A. Khademhosseini, R. Langer, *Biomaterials* **2007**, *28*, 5087.

[46] C. Paquet, Z. J. Jakubek, B. Simard, *ACS Appl. Mater. Interfaces* **2012**, *4*, 4934.
[47] M. Ren, W. Guo, H. Guo, X. Ren, *ACS Appl. Mater. Interfaces* **2019**.
[48] S. Seiffert, *Macromol. Chem. Phys.* **2017**, *218*, 1600280.
[49] R. K. Shah, H. C. Shum, A. C. Rowat, D. Lee, J. J. Agresti, A. S. Utada, L. Y. Chu, J. W. Kim, A. Fernandez-Nieves, C. J. Martinez, *Mater. Today* **2008**, *11*, 18.
[50] S. Jockusch, N. J. Turro, Y. Mitsukami, M. Matsumoto, T. Iwamura, T. Lindner, A. Flohr, G. di Massimo, *J. Appl. Polym. Sci.* **2009**, *111*, 2163.
[51] F. L. Buchholz, S. C. Sutie, P. B. Smith, R. E. Reim, A. T. Graham, in *Modern Superabsorbent Polymer Technology* (Eds: F. L. Buchholz, A. T. Graham), Wiley-VCH, New York **1998**, Chs. 4 and 5.
[52] T. Tanaka, D. J. Fillmore, *J. Chem. Phys.* **1979**, *70*, 1214.
[53] Standard Practice for the Preparation of Substitute Ocean Water, ASTM International, West Conshohocken, PA **2013**, https://www.astm.org/Standards/D1141.htm.
[54] M. Mussel, P. J. Basser, F. Horkay, *Soft Matter* **2019**, *15*, 4153.
[55] T. Q. Bui, V. D. Cao, N. B. D. Do, T. E. Christoffersen, W. Wang, A. L. Kjøniksen, *ACS Appl. Mater. Interfaces* **2018**, *10*, 22218.